AAC Accepted Manuscript Posted Online 5 August 2020
Antimicrob. Agents Chemother. doi:10.1128/AAC.00825-20
Copyright © 2020 American Society for Microbiology. All Rights Reserved.

Atazanavir, alone or in combination with ritonavir, inhibits SARS-CoV-2 replication and pro-inflammatory cytokine production

Running-title: SARS-CoV-2 is susceptible to atazanavir

Natalia Fintelman-Rodrigues[1,9#], Carolina Q. Sacramento[1,9#], Carlyle Ribeiro Lima[9,#], Franklin Souza da Silva[2,9], André C. Ferreira[1,3,9], Mayara Mattos[1,9], Caroline S. de Freitas[1,9], Vinicius Cardoso Soares[1], Suelen da Silva Gomes Dias[1], Jairo R. Temerozo[4,5], Milene D. Miranda[6], Aline R. Matos[6], Fernando A. Bozza[7,8], Nicolas Carels[9], Carlos Roberto Alves[2], Marilda M. Siqueira[6], Patrícia T. Bozza[1], Thiago Moreno L. Souza[1,9,*]

# - These authors contributed equally to this work, Author order was determined alphabetical order by their surname

1 – Laboratório de Imunofarmacologia, Instituto Oswaldo Cruz (IOC), Fundação Oswaldo Cruz (Fiocruz), Rio de Janeiro, RJ, Brazil.

2 – Laboratório de Biologia Molecular e Doenças Endêmicas, IOC, Fiocruz, Rio de Janeiro, RJ, Brazil.

3 – Universidade Iguaçu, Nova Iguaçu, RJ, Brazil.

4 – Laboratório de Pesquisas sobre o Timo, IOC, Fiocruz, Rio de Janeiro, RJ, Brazil.

5 - National Institute for Science and Technology on Neuroimmunomodulation (INCT/NIM), IOC, Fiocruz, Rio de Janeiro, RJ, Brazil.

6 – Laboratório de Vírus Respiratório e do Sarampo, IOC, Fiocruz, Rio de Janeiro, RJ, Brazil.

7 – Instituto Nacional de Infectologia Evandro Chagas, Fiocruz, Rio de Janeiro, RJ, Brazil

8 – Instituto D'or de Pesquisa e Ensino, Rio de Janeiro, RJ, Brazil

9 - National Institute for Science and Technology on Innovation in Diseases of Neglected Populations (INCT/IDPN), Center for Technological Development in Health (CDTS), Fiocruz, Rio de Janeiro, RJ, Brazil.

***Correspondence footnote:**

Thiago Moreno L. Souza, PhD

****

Fundação Oswaldo Cruz (Fiocruz)
Centro de Desenvolvimento Tecnológico em Saúde (CDTS)
Instituto Oswaldo Cruz (IOC)
Pavilhão Osório de Almeida, sala 16
Av. Brasil 4365, Manguinhos, Rio de Janeiro - RJ, Brasil, CEP 21060340
Tel.: +55 21 2562-1311
Email: tmoreno@cdts.fiocruz.br

AAC

Abstract

Severe acute respiratory syndrome coronavirus 2 (SARS-CoV-2) is already responsible for far more deaths than previous pathogenic coronaviruses (CoVs) from 2002 and 2012. The identification of clinically approved drugs to be repurposed to combat 2019 CoV disease (COVID-19) would allow the rapid implementation of potentially life-saving procedures. The major protease (Mpro) of SARS-CoV-2 is considered a promising target, based on previous results from related CoVs with lopinavir (LPV), an HIV protease inhibitor. However, limited evidence exists for other clinically approved antiretroviral protease inhibitors. Extensive use of atazanavir (ATV) as antiretroviral and previous evidence suggesting its bioavailability within the respiratory tract prompted us to study this molecule against SARS-CoV-2. Our results show that ATV could dock in the active site of SARS-CoV-2 Mpro, with greater strength than LPV, blocking Mpro activity. We confirmed that ATV inhibits SARS-CoV-2 replication, alone or in combination with ritonavir (RTV) in Vero cells and human pulmonary epithelial cell line. ATV/RTV also impaired virus-induced enhancement of IL-6 and TNF-α levels. Together, our data strongly suggest that ATV and ATV/RTV should be considered among the candidate repurposed drugs undergoing clinical trials in the fight against COVID-19.

AAC

1) Introduction

Coronaviruses (CoVs) are single-stranded positive sense RNA viruses able to infect a range of hosts, from animals and humans (1). At the beginning of the 21st century, highly pathogenic CoVs emerged, the severe acute respiratory syndrome (SARS-CoV), middle-east respiratory syndrome (MERS-CoV) (2), and, at the end of 2019, a novel variant of SARS-CoV (SARS-CoV-2) (3). SARS-CoV-2 has spilled over to humans from animal reservoirs, most likely bats and/or pangolins (3). Both SARS- and MERS-CoV raised international public health concerns with rates of mortality of 10 and 35 %, respectively (4, 5). SARS-CoV-2 became a pandemic threat and provoked 5-10 % mortality, resulting in more than 600 thousands deaths in 7 months (6).

Currently, the most effective response to the SARS-CoV-2 pandemic has been social distancing, to avoid contact between infected and uninfected individuals and flatten the virus dissemination curve. While these social actions can disrupt virus transmission rates, they are not expected to reduce the absolute number of infected individuals. Furthermore, these strategies are also provoking a severe reduction in global economic activity (7). To effectively combat the impact of SARS-CoV-2 on infected individuals, and society as a whole, it is essential to identify antiviral drugs for immediate use, as well as develop new drugs and a vaccine for long-term solutions to the disease associated with SARS-CoV-2 (COVID-19).

Repurposing of clinically approved drugs is the fastest pathway to identify therapeutics (8). Some of the most promising antiviral candidates against SARS-CoV-2 have been under investigation since the outbreak of SARS-CoV in 2002. Building on this continuous investigation, an unprecedented effort from World Health Organization (WHO)

AAC

to run a global clinical trial, called Solidarity, is ongoing (9). This mega trial has been putting forward lopinavir (LPV)/ritonavir (RTV), in combination or not with interferon-β (IFN-β), chloroquine (CQ) and remdesivir to treat COVID-19 (9). Some of the arms of the Solidarity trial are under reavaluation, due to limited clinical benefits of CQ and LPV/RTV (9–11). Thus, other antiviral candidates must be evaluated from a pre-clinical perspective.

The most successful antiviral drugs often directly target viral enzymes (12). For CoVs, its major protease (Mpro) has been a promising drug target for almost two decades, starting with early studies on 2002 SARS-CoV that showed this enzyme to be inhibited by LPV/RTV, inhibitors of HIV protease (13). Mpro is required during the CoV replication cycle to process viral polyprotein (14). Highly pathogenic CoVs contain two open reading frames, ORF1a and ORF1b, that are translated by host ribosomes into their two respective viral polyproteins, pp1a and pp1ab. ORF1a encodes two cysteine proteases, the papain-like protease (PLpro) and Mpro. While PLpro cuts the polyprotein at three sites, Mpro is responsible for cleavage at 11 another locations that, together, produce the 16 nonstructural proteins.

In a combined therapy of LPV with RTV, LPV is included as the principle antiviral compound and RTV as an inhibitor drug metabolism, being a specific inhibitor of the cytochrome p450, CYP3A4 isoform (15). In the early 2000s, another contemporary antiretroviral protease inhibitor, atazanavir (ATV), replaced LPV due to fewer side effects for the patients (16, 17). Contemporarily, *in silico* evidence suggested that other HIV protease inhibitors would target SARS-CoV-2 Mpro better than LPV, that included ATV (18). Importantly, ATV has been described to reach the lungs after intravenous

AAC

administration (19)(20). Moreover, a proposed secondary use of ATV to treat pulmonary fibrosis suggested that this drug could functionally reach the lungs (20).

The seriousness of COVID-19 and the need for an immediate oral intervention, along with this series of observations with HIV protease inhibitors, motivated us to evaluate the susceptibility of SARS-CoV-2 to ATV. Since ATV is available as a clinical treatment alone or in combination with RTV, both therapies were studied. For the first time, we describe that SARS-CoV-2 Mpro is a target for ATV, which alone or with RTV could inhibit viral replication and prevent the release of cytokine storm-associated mediators. Our timely data highlights an additional therapeutic approach against COVID-19 that should be considered for clinical trials with another protease inhibitor, which is superior to LPV *in vitro*.

2) Results

2.1) ATV docks into SARS-CoV-2 Mpro more spontaneously and stably than LPV

SARS-CoV-2 enzyme Mpro (PDB:6LU7) supports the docking by both ATV and LPV (Figure S1 e S2). ATV and LPV occupy S1*, and S2 cleft of their active site with free energy scores of -59.87 and -65.49 Kcal/mol, respectively (Figure S1 and S2). ATV bound more spontaneously because of its hydrogens bonds with Mpro, whereas LPV depends on hydrophobic interactions (Figure S2).

Molecular dynamic analysis revealed that the root-mean-square deviation (RMSD) for the SARS-CoV-2 Mpro backbone presented different conformations in complex with ATV or LPV (Figure S3). LPV was initially at a 3.8 Å distance from the catalytic residue Cys145 (Figure S4A and S5A). After conformational changes, LPV was 7,17 Å distant from active site (Figure 1A and 1C), likely limiting its antiviral activity. Another critical residue, His41, was satisfactorily at a distance of 2.89 Å from bound LPV (Figure 1A and 1C). ATV neither interacts with His41 nor Cys145, at initial analysis (Figure S4B and S5B). Nevertheless, ATV´s position remained stable within the active site independently of conformational changes (Figure 1B and 1D). The steric occupation of the cleft in the enzymatic active site by ATV, which block the residues of the catalytic amino acids, can be explained by its stronger interactions with Mpro, compared to LPV (Tables S1-S3).

2.2) ATV inhibits SARS-CoV-2 Mpro enzymatic activity

Next, we evaluated whether ATV could inhibit SARS-CoV-2 Mpro activity by partially purifying the enzyme in cellular fractions obtained from SARS-CoV-2-infected cells and performing zymographic profiles. To assure that the proteinase profiles were not dependent on cellular enzymes, similar fractions of mock-infected cells were also prepared. The results from cysteine proteinase zymographic profiles in gelatinolytic gels reveled a cellular related band of approximately 70 kDa under both conditions (Figure 2, lanes Nil). This activity was blocked by the drug E-64, an epoxide that acts as an irreversible inhibitor of cysteine proteases (Figure 2, lanes E-64). In the infected cells, a region of activity was observed between 31 and 38 kDa that was not present in the mock fraction (Figure 2). This zone of molecular weight is consistent with expected size of SARS-CoV-2 Mpro. The enzyme activity was inhibiter by exposure of the gels to 10 µM of ATV, without affecting cellular cysteine proteinase (Figure 2, lanes ATV). As a control the activity of SARS-CoV-2 Mpro in fractions from infected cells was evaluated by treatment with RTV, which inhibited activity in the molecular range of 31-38 kDa without a change in the 70 kDa

AAC

AAC

region (Figure 2, lanes RTV). These data are consistent with predictions from the molecular modeling and dynamics that ATV targets SARS-CoV-2 Mpro.

2.3) SARS-CoV-2 is susceptible to ATV and ATV/RTV in different cell types

We extended our investigation to evaluate the susceptibility of SARS-CoV-2 to ATV using in different cellular systems. Vero cells are a well-known model to produce high virus titers. ATV alone, or in combination with RTV, decreased infectious virus production and RNA levels this cell lines (Figure 3A and B, respectively). ATV/RTV was more potent than ATV, with EC_{50} values of 0.5 ± 0.08 µM and 2.0 ± 0.12 µM, respectively (Figure 3B). Positive controls, CQ, LPV/RTV and remdesivir displayed potencies of 1.0 ± 0.07 µM, 5.3 ± 0.5 µM and 0.5 ± 0.08 µM, respectively (Figure 3B). Our positive controls display consistent with results in the literature (21), validating our analysis. The ATV/RTV, ATV, CQ, LPV/RTV and remdesivir cytotoxicity values, CC_{50}, were 280 ± 3 µM, 312 ± 8 µM, 259 ± 5 µM, 91 ± 3 µM and 512 ± 30 µM, respectively. Our results indicate that the selectivity index (SI, which represents the ratio between the CC_{50} and EC_{50} values) for ATV/RTV, ATV, CQ, LPV/RTV and remdesivir were 560, 156, 259, 18 and 1020, respectively, which shows that ATV/RTV and ATV have therapeutic potential above CQ and LPV/RTV, compounds that advanced towards clinical trials early after the pandemic outbreak.

Since the results regarding the pharmacologic activity of ATV and ATV/RTV against SARS-CoV-2 replication in Vero cells were promising, we next investigated whether the proposed drug therapies could inhibit virus replication in a human epithelial pulmonary cell line (A549). ATV alone showed a nearly 10-fold increase in potency for inhibiting SARS-CoV-2 replication in A549 (Figure 3C) compared to Vero cells (Figure 3B). ATV/RTV and

CQ were similarly potent in inhibiting virus replication in both cell types (Figure 3B and C). Drugs repurposed in this study, ATV and ATV/RTV were more potent than positive controls to inhibit SARS-CoV-2 replication in A549 cells. Potencies for ATV/RTV, ATV, CQ, LPV/RTV and remdesivir were 0.60 ± 0.05 µM, 0.22 ± 0.02 µM, 0.89 ± 0.02 µM, 0.9 ± 0.5 µM and 0.6 ± 0.02 µM, respectively. *In vitro* results confirmed the rational that SARS-CoV-2 would be susceptible to ATV that included cells derived from the respiratory tract.

2.4) **ATV and ATV/RTV prevent cell death and pro-inflammatory cytokine production in SARS-CoV-2-infected monocytes.**

Severe COVID-19 has been associated with levels of lactate dehydrogenase (LDH), interleukin 6 (IL-6) and leukopenia(22). Viral infection in the respiratory tract often trigger the migration of blood monocytes to orchestrate the transition from innate to adaptive immune responses(23). For these reasons, ATV and ATV/RTV were tested at suboptimal (1 µM) or optimal (10 µM) doses, with respect to their *in vitro* pharmacological parameter against SARS-CoV-2.

ATV/RTV, CQ and remdesivir were similarly efficient to reduce the amount viral genome equivalent in the human monocytes (Figure 4A). Virus infection increased cellular mortality by 75%, which was prevented by ATV, ATV/RTV and remdesivir (Figure 4B). LPV/RTV was inefficient to reduce viral RNA levels and cell death (Figure 4A and 4B). Moreover, we observed that infections by SARS-CoV-2 triggered the expected increase in the IL-6 levels in the culture supernatant, which ranged from 20- to 60-fold depending on the cell donor (Figure 4C). The virus-induced enhancement of IL-6 levels were

AAC

significantly prevented by treatment with ATV, ATV/RTV and CQ (Figure 4C). Another biomarker of uncontrolled pro-inflammatory cytokine response, TNF-α, was up-regulated 40-fold during virus infection (Figure 4D). ATV, ATV/RTV and remdesivir (10 µM) could significantly prevent the induction of TNF-α release (Figure 4D). Altogether, our results confirm that ATV and ATV/RTV should not be ignored as an additional therapeutic option against COVID-19.

3) Discussion

In these two decades of the 21st century, the human vulnerability to emerging viral diseases has been notable (24). The emergence of infectious disease highlights the undeniable fact that existing countermeasures are inefficient to prevent virus spill over and diseases outbreak. Preclinical data on the susceptibility of an emerging virus to clinically approved drugs can allow for the rapid mobilization of resources towards clinical trials (8). This approach proved feasible for combating the Zika, yellow fever and chikungunya outbreaks experienced in Brazil over the past 5 years, when our group demonstrated that sofosbuvir, a blockbuster drug against hepatitis C, could represent a compassionate countermeasure against these diseases (25–29).

Currently, the rate of SARS-CoV-2 dissemination has become one of the most rapidly evolving pandemics known in modern times with the number of cases and deaths doubling every week and the peak of the pandemic has yet to arrive in some territories (6). The existence of several ongoing clinical trials against COVID-19 reinforces the suggestion that drug repurposing represents the fastest approach to identify therapies to emerging infectious disease (8).

AAC

Among therapies initially included in the Solidarity trial, most interest results come from remdesivir, whereas CQ and LPV/RTV showed limited clinical benefit (9). LPV/RTV reduced mortality in critically patients by 5 % (11). On the other hand, this therapy showed no clinical clinical benefit in a large clinical trial (30). Although the combination therapy with protease (LPV/RTV), RNA polymerase (Ribavirin) and immunomodulators (IFN-β) reduced the viral loads of COVID-19 patients (31), these drugs seem to be unpractical for early treatment – because of IFN's price safety profile. The history of antiretroviral research teaches us that combinations are necessary. Positive laboratory and clinical results with RNA polymerase inhibitors, such as remdesevir, ribavirin and favipiravir (21, 31, 32), against SARS-CoV-2 could be more effective if combined with active protease inhibitors. We highlight ATV and ATV/RTV because: i) our assay read out to quantify infections virus particles revels a good profile of antiviral activity; ii) higher potencies respiratory cells and iii) ability to reduce pro-inflammation mediator levels in monocytes.

We interpret that early repurposing LPV/RTV for COVID-19 was based on previous evidence during the SARS-CoV outbreak in 2002 and again for MERS-CoV (33). Information on the susceptibility of SARS-CoV-2 to other antiviral protease inhibitors approved since 2003, such as ATV, has been scarce. Since this year, ATV become a wider prescribed drug among HIV-infected individuals, than LPV, including for critically ill patients (17). ATV shows a safer profile than LPV in both short- and long-term therapeutic regimens (16, 34). ATV has a documented bioavailability to reach the respiratory tract(19, 35), which lead to its proposed use against pulmonary fibrosis (20). Under our experimental conditions, ATV was superior to LPV/RTV, which may motivate further clinical trials.

AAC

The potencies of LPV/RTV against SARS-CoV-2 was lower compared to ATV and ATV/RTV. Nevertheless, remdesevir was more potent than ATV or ATV/RTV. The improved potency of ATV, in comparison to LPV, may be at least in part due to its multiple hydrogen bond driven interactions within the Mpro active site. Other investigators have also recognized a wider range of interactions of ATV and Mpro compared to LPV (18, 36), although none provided functional evidence through phenotypic assays as presented here. Neither ATV nor LPV displayed any interactions with the catalytic dyad of Cys145 and His41 at the start of the molecular dynamic simulations. However, important interactions were observed at its end, such as LPV-His41 and ATV-Glu166. Glu166 is one of the residues that promotes the opening of Mpro for its substrate to interact with the active site (37, 38).

Highly pathogenic respiratory viruses, such as influenza A virus, have been associated with a cytokine storm that describes an uncontrolled pro-inflammatory cytokine response (39, 40). Cytokine storms also seem to be highly relevant for pathogenic human CoVs(41). Contemporary investigations on SARS-CoV-2 strongly suggest the involvement of cytokine storm with disease severity (22). COVID-19 mortality is associated with enhanced IL-6 levels and consistent cell death, as measured by LDH release (22). We showed that ATV and ATV/RTV decreased IL-6 release in SARS-CoV-2-infected human primary monocytes. Moreover, we also included in our analysis TNF-α, another hallmark of inflammation during respiratory virus infections (22, 43). Our results reveled that cellular mortality and cytokine storm-associated mediators were reduced after treatment with the repurposed antiretroviral drugs used in this study.

AAC

As the SARS-CoV-2 pandemic goes on and the Solidarity trials fail to demonstrate benefit of LPV/RTV, pre-clinical data or clinically approved protease inhibitors, such as ATV-ATV/RTV, need to be catalogued. Higher potency of ATV-ATV/RTV over LPV/RTV is the contribution of our study to highlight a new option among clinically approved drugs that should be considered in ongoing clinical trials for an effective treatment for COVID-19.

Material and Methods

4.1. Reagents.

The antiviral ATV, ATV/RTV and CQ were received as donations from Instituto de Tecnologia de Fármacos (Farmanguinhos, Fiocruz). ATV/RTV was prepared in the proportion of 3:1 as the pharmaceutical pills are composed of 300 mg ATV and 100 mg RTV daily. Remdesivir and LPV/RTV (4:1 ratio) were purchased from https://www.selleckchem.com/. ELISA assays were purchased from R&D Bioscience. All small molecule inhibitors were dissolved in 100% dimethylsulfoxide (DMSO) and subsequently diluted at least 10^4-fold in culture or reaction medium before each assay. The final DMSO concentrations showed no cytotoxicity. The materials for cell culture were purchased from Thermo Scientific Life Sciences (Grand Island, NY), unless otherwise mentioned.

Triton X-100 (TX-100), 3-[(3-Cholamidopropyl)dimethylammonio]-1-propanesulfonate hydrate (CHAPS), 1,2,3-Propanetriol (glycerol), bovine serum albumin (BSA), Phosphate-buffered saline (PBS), N-benzyloxycarbonyl-l-phenylalanyl-l-arginine 7-amino-4-methylcoumarin (Z-FR-AMC; $\varepsilon = 1.78 \times 10^4$ M^{-1} cm^{-1}), dithiothreitol (DTT) and trans-

AAC

epoxysuccinyl-l-leucylamido(4-guanidino)butane (E-64) were purchased from Sigma Aldrich Chemical Co. (St. Louis, MO, USA). HiTrap Q FF anion exchange chromatography column (HiTrap Q FF) was purchase from GE Healthcare Life Sciences. Micro-bicinchoninic acid (BCA) protein assay kit was purchased from Pierce Chemical Co. (Appleton, WI). All other reagents were of analytical grade or better.

4.2. Cells and Virus

African green monkey kidney (Vero, subtype E6) and A549 (human lung epithelial cells) cells were cultured in high glucose DMEM with 10% fetal bovine serum (FBS; HyClone, Logan, Utah), 100 U/mL penicillin and 100 μg/mL streptomycin (Pen/Strep; ThermoFisher) at 37 °C in a humidified atmosphere with 5% CO_2.

Human primary monocytes were obtained after 3 h of plastic adherence of peripheral blood mononuclear cells (PBMCs). PBMCs were isolated from healthy donors by density gradient centrifugation (Ficoll-Paque, GE Healthcare). PBMCs (2.0×10^6 cells) were plated onto 48-well plates (NalgeNunc) in RPMI-1640 without serum for 2 to 4 h. Non-adherent cells were removed and the remaining monocytes were maintained in DMEM with 5% human serum (HS; Millipore) and penicillin/streptomycin. The purity of human monocytes was above 95%, as determined by flow cytometric analysis (FACScan; Becton Dickinson) using anti-CD3 (BD Biosciences) and anti-CD16 (Southern Biotech) monoclonal antibodies.

SARS-CoV-2 was prepared in Vero E6 cells from an isolate contained on a nasopharyngeal swab obtained from a confirmed case in Rio de Janeiro, Brazil. Viral experiments were performed after a single passage in a cell culture in a 150 cm^2 flasks with

AAC

DMEM plus 2% FBS. Observations for cytopathic effects were performed daily and peaked 4 to 5 days after infection. All procedures related to virus culture were handled in a biosafety level 3 (BSL3) multiuser facility according to WHO guidelines. Virus titers were determined as the tissue culture infectious dose at 50% ($TCID_{50}$/mL). Virus stocks were kept in - 80 °C ultralow freezers.

The virus strain was sequenced to confirm the virus identity and its complete genome is publicly deposited (https://nextstrain.org/ncov: Brazil/RJ-314/2020 or GISAID EPI ISL #414045).

4.3. Cytotoxicity assay

Monolayers of 1.5 x 10^4 Vero cells in 96-well plates were treated for 3 days with various concentrations (semi-log dilutions from 600 to 10 µM) of ATV, ATV/RTV or CQ. Then, 5 mg/ml 2,3-bis-(2-methoxy-4-nitro-5-sulfophenyl)-2*H*-tetrazolium-5-carboxanilide (XTT) in DMEM was added to the cells in the presence of 0.01% of N-methyl dibenzopyrazine methyl sulfate (PMS). After incubating for 4 h at 37 °C, the plates were measured in a spectrophotometer at 492 nm and 620 nm. The 50% cytotoxic concentration (CC_{50}) was calculated by a non-linear regression analysis of the dose–response curves.

4.4. Yield-reduction assay

Cells were infected with a multiplicity of infection (MOI) of 0.01. Vero or A549 cells were infected at densities of 5 x 10^5 cells/well. Human primary monocytes were infected at density of 2-8 x 10^5 cells/well, depending on the endogenous characteristic of the cell donor. Infections were performed in 48-well plates for 2h at 37 °C. The cells were washed, and various concentrations of compounds were added to DMEM with 2% FBS. After 48h,

AAC

virus in the supernatants were quantified by real time RT-PCR and/or by $TCID_{50}$/mL. A variable slope non-linear regression analysis of the dose-response curves was performed to calculate the concentration at which each drug inhibited the virus production by 50% (EC_{50}).

4.5. Virus titration

Monolayers of Vero cells (2 x 10^4 cell/well) in 96-well plates were infected with a log-based dilution of supernatants containing SARS-CoV-2 for 1h at 37°C. Cells were washed, fresh medium added with 2% FBS and 3 to 5 days post infection the cytopathic effect was scored in at least 10 replicates per dilution by independent readers. The reader was blind with respect to source of the supernatant. A Reed and Muench scoring method was employed to determine $TCID_{50}$/mL(43).

4.6. Molecular detection of virus RNA levels.

The total RNA from the supernatants culture was extracted using QIAamp Viral RNA (Qiagen®), according to manufacturer’s instructions. Quantitative RT-PCR was performed using QuantiTect Probe RT-PCR Kit (Quiagen®) in an ABI PRISM 7500 Sequence Detection System (Applied Biosystems). Amplifications were carried out in 25 µL reaction mixtures containing 2× reaction mix buffer, 50 µM of each primer, 10 µM of probe, and 5 µL of RNA template. Primers, probes, and cycling conditions recommended by the Centers for Disease Control and Prevention (CDC) protocol were used to detect the SARS-CoV-2(44). The standard curve method was employed for virus quantification. For reference to the cell amounts used, the housekeeping gene RNAse P was amplified. The Ct values for

AAC

this target were compared to those obtained to different cell amounts, 10^7 to 10^2, for calibration.

4.7. Measurements Inflammatory Mediators and cell death marker

The levels of TNF-α, IL-6 and LDH were quantified in the monocyte supernatants from infected and uninfected cells. ELISA for TNF-α and IL-6 required 100 μL of supernatants to be exposed to capture antibody in 96-well plates. After a 2h incubation period at room temperature (RT), the detection antibody was added. Plates were incubated for another 2h at RT. Streptavidin-HRP and its substrate were added, incubated for 20 minutes and the optical density was determined using a microplate reader set to 450 nm.

Extracellular lactate dehydrogenase (LDH) was quantified using Doles® kit according to manufacturer's` instructions. Supernatant was centrifuged at 5,000 rpm for 1 minute, to remove cellular debris. A total of 25 μL of supernatant was placed into 96-well plates and incubated with 5 μL of ferric alum and 100 μL of LDH substrate for 3 minutes at 37 °C. Nicotinamide adenine dinucleotide (NAD, oxidized form) was added followed by the addition of a stabilizing solution. After a 10 min incubation, plates were measured in a spectrophotometer at 492 nm.

4.8. Molecular docking

ATV (PubChem CID: 148192) and LPV (PubChem CID: 92727) were used as inhibitors of the SARS-CoV-2 Mpro. ATV and LPV were prepared using the Generalized Amber Force Field (GAFF) and their charges were obtained using the AM1-BCC loading scheme (45, 46).

AAC

Molecular docking experiments were performed with DOCK 6.9(47) for identifying the binding site of the Mpro. SARS-CoV-2 Mpro structure was obtained from Protein Data Bank (RCSB PDB, http://www.rcsb.org), under the accession code #6LU7 (48). The active site region was identified by using a complexed peptide (N-[(5-methylisoxazol-3-yl)carbonyl]alanyl-l-valyl-n~1~-((1r,2z)-4-(benzyloxy)-4-oxo-1-{[(3r)-2-oxopyrrolidin-3-yl]methyl}but-2-enyl)-l-leucinamide) as a guide. The creation of the DOCK 6.9 input files for docking was performed using Chimera 1.14(49).

The docking of ligands was performed in a box of 10 Å edges with its mass center matching that of the complexed peptide. Each scan produced 20 conformations for each ligand with the best score being used for molecular dynamics simulations.

4.9. Molecular dynamics

Since the tertiary structure (3D) of the SARS-CoV-2 Mpro is a homodimer, we focused the molecular dynamics only one chain, henceforward chain A. Molecular dynamics calculations were performed using NAMD 2.9(50) and Charmm27* force field(51) at pH 7, i.e., with deprotonated Glu and Asp, protonated Arg and Lys, and neutral His with a protonated Nε atom. This all-atom force field has been able to fold properly many soluble proteins(52–54). The soluble proteins were centered in a cubic box of TIP3P water molecules(55); the box extended 1.2 nm outside the protein on its four lateral sides, and the appropriate numbers of Na+ and Cl- ions were added to ensure system neutralization. The electrostatic interactions were calculated using the Particle Mesh Ewald method and a cutoff of 1.2 nm(56). The same cutoff of 1.2 nm was used for the Van der Waals interactions. The non-bonded pair lists were updated every 10 fs. In what follows, the analysis is based on MD simulation of 100 ns at 310 K.

AAC

4.10. Protein extraction

Protein extracts containing SARS-CoV-2 Mpro activity were obtained from Vero cell monolayers at 25 cm^2 flasks that were infected for 1h with an MOI of 0.1 at 37 °C and 5% CO_2. After 1 or 2 days of infection, the supernatant was harvested and monolayers were washed 3 times with in sterile cold PBS (pH 7.2). Next, cells were suspended into 1 mL of lysis buffer (100 mM Tris-HCl (pH 8.0), 150 mM NaCl, 10% glycerol and 0.6% Triton X-100) and kept at 4 °C. The soluble protein fraction was isolated as the supernatant after centrifugation (100,000 x g, 30 min, 4 °C) and stored at -20°C until further use. The protein concentrations of the samples were determined using the BCA protein assay kit.

4.11. Zymographic assays

Proteinases were assayed after electrophoresis on 10% SDS-PAGE with 0.1% copolymerized gelatin(57). Briefly, the gels were loaded per slot with 12 µg of soluble proteins dissolved in Laemmli's buffer, and following electrophoresis at a constant voltage of 200 V at 4°C, they were soaked for 1 h at 25 °C in washing buffer (0.1 mM sodium acetate buffer (pH 5.5) containing 2.5% TX-100). Proteinase activity was detected by incubating (16 h at 37 °C) the gels in reaction buffer (0.1 mM sodium acetate buffer pH 5.5 containing 1.0 mM DTT), in the presence and absence of same concentration of 10 µM of E-64, ATV, RTV or the ATV/RTV combination. Hydrolysis of gelatin was visualized by staining the gels with amido black 0.2%(58).

4.12. Statistical analysis

The assays were performed blinded by one professional, codified and then read by another professional. All experiments were carried out at least three independent times,

AAC

including a minimum of two technical replicates in each assay. The dose-response curves used to calculate EC_{50} and CC_{50} values were generated by variable slope plot from Prism GraphPad software 8.0. The equations to fit the best curve were generated based on R^2 values ≥ 0.9. Student's T-test was used to access statistically significant P values <0.05. The statistical analyses specific to each software program used in the bioinformatics analysis are described above.

Acknowledgments

Thanks are due to Dr. Carmen Beatriz Wagner Giacoia Gripp for assessments related to BSL3 facility. This work was supported by Conselho Nacional de Desenvolvimento Científico e Tecnológico (CNPq), Fundação de Amparo à Pesquisa do Estado do Rio de Janeiro (FAPERJ). This study was financed in part by the Coordenação de Aperfeiçoamento de Pessoal de Nível Superior - Brasil (CAPES) - Finance Code 001. Funding was also provided by CNPq, CAPES and FAPERJ through the National Institutes of Science and Technology Program (INCT) to Carlos Morel (INCT-IDPN). Thanks are due to Oswaldo Cruz Foundation/FIOCRUZ under the auspicious of Inova program. The funding sponsors had no role in the design of the study; in the collection, analyses, or interpretation of data; in the writing of the manuscript, and in the decision to publish the results.

AAC

References

1. Masters PS. 2006. The molecular biology of coronaviruses. Adv Virus Res 66:193–292.

2. Cui J, Li F, Shi Z-L. 2019. Origin and evolution of pathogenic coronaviruses. Nat Rev Microbiol 17:181–192.

3. Lam TT-Y, Shum MH-H, Zhu H-C, Tong Y-G, Ni X-B, Liao Y-S, Wei W, Cheung WY-M, Li W-J, Li L-F, Leung GM, Holmes EC, Hu Y-L, Guan Y. 2020. Identifying SARS-CoV-2 related coronaviruses in Malayan pangolins. Nature 583: 282-285.

4. WHO, World Health Organization | Middle East respiratory syndrome coronavirus (MERS-CoV). 2020, https://www.who.int/emergencies/mers-cov/en/, accessed on 24-Jul-2020.

5. WHO, World Health Organization | Severe Acute Respiratory Syndrome (SARS). 2020, https://www.who.int/health-topics/severe-acute-respiratory-syndrome, accessed on 24-jul-2020.

6. Dong E, Du H, Gardner L. 2020. An interactive web-based dashboard to track COVID-19 in real time. Lancet Infect Dis 20: 533-534.

7. Romer P, Garber AM. 2020. Opinion | Will Our Economy Die From Coronavirus? N Y Times, https://www.nytimes.com/2020/03/23/opinion/coronavirus-depression.html, accessed on 24-jul-2020.

AAC

8. Harrison C. 2020. Coronavirus puts drug repurposing on the fast track. Nat Biotechnol 38: 379-381.

9. WHO, World Health Organization | WHO R&D Blueprint: informal consultation on prioritization of candidate therapeutic agents for use in novel coronavirus 2019 infection, Geneva, Switzerland, 24 January 2020. WHO/HEO/R&D Blueprint (nCoV)/2020.1, https://apps.who.int/iris/handle/10665/330680, accessed on 24-jul-2020.

10. Borba MGS, Val FFA, Sampaio VS, Alexandre MAA, Melo GC, Brito M, Mourão MPG, Brito-Sousa JD, Baía-da-Silva D, Guerra MVF, Hajjar LA, Pinto RC, Balieiro AAS, Pacheco AGF, Santos JDO, Naveca FG, Xavier MS, Siqueira AM, Schwarzbold A, Croda J, Nogueira ML, Romero GAS, Bassat Q, Fontes CJ, Albuquerque BC, Daniel-Ribeiro C-T, Monteiro WM, Lacerda MVG. 2020. Effect of High vs Low Doses of Chloroquine Diphosphate as Adjunctive Therapy for Patients Hospitalized With Severe Acute Respiratory Syndrome Coronavirus 2 (SARS-CoV-2) Infection: A Randomized Clinical Trial. JAMA Netw Open 3:e208857–e208857.

11. Cao B, Wang Y, Wen D, Liu W, Wang J, Fan G, Ruan L, Song B, Cai Y, Wei M, Li X, Xia J, Chen N, Xiang J, Yu T, Bai T, Xie X, Zhang L, Li C, Yuan Y, Chen H, Li H, Huang H, Tu S, Gong F, Liu Y, Wei Y, Dong C, Zhou F, Gu X, Xu J, Liu Z, Zhang Y, Li H, Shang L, Wang K, Li K, Zhou X, Dong X, Qu Z, Lu S, Hu X, Ruan S, Luo S, Wu J, Peng L, Cheng F, Pan L, Zou J, Jia C, Wang J, Liu X, Wang S, Wu X, Ge Q, He J, Zhan H, Qiu F, Guo L, Huang C, Jaki T, Hayden FG, Horby PW, Zhang D, Wang C. 2020. A Trial of Lopinavir-Ritonavir in Adults Hospitalized with Severe Covid-19. N Engl J Med 382: 1787-1799.

12. De Clercq E, Li G. 2016. Approved Antiviral Drugs over the Past 50 Years. Clin Microbiol Rev 29:695–747.

13. Wu C-Y, Jan J-T, Ma S-H, Kuo C-J, Juan H-F, Cheng Y-SE, Hsu H-H, Huang H-C, Wu D, Brik A, Liang F-S, Liu R-S, Fang J-M, Chen S-T, Liang P-H, Wong C-H. 2004. Small molecules targeting severe acute respiratory syndrome human coronavirus. Proc Natl Acad Sci U S A 101:10012–10017.

14. Fehr AR, Perlman S. 2015. Coronaviruses: an overview of their replication and pathogenesis. Methods Mol Biol Clifton NJ 1282:1–23.

15. Gong Y, Haque S, Chowdhury P, Cory TJ, Kodidela S, Yallapu MM, Norwood JM, Kumar S. 2019. Pharmacokinetics and pharmacodynamics of cytochrome P450 inhibitors for HIV treatment. Expert Opin Drug Metab Toxicol 15:417–427.

16. Stanley TL, Joy T, Hadigan CM, Liebau JG, Makimura H, Chen CY, Thomas BJ, Weise SB, Robbins GK, Grinspoon SK. 2009. Effects of Switching from Lopinavir/ritonavir to Atazanavir/ritonavir on Muscle Glucose Uptake and Visceral Fat in HIV Infected Patients. AIDS Lond Engl 23:1349–1357.

17. Gibert CL. 2016. Treatment Guidelines for the Use of Antiretroviral Agents in HIV-Infected Adults and Adolescents: An Update. Fed Pract 33:31S-36S.

18. Dayer MR. Old Drugs for Newly Emerging Viral Disease, COVID-19: Bioinformatic Prospective. https://arxiv.org/abs/2003.04524, accessed on 24-jul-2020

19. Gautam N, Roy U, Balkundi S, Puligujja P, Guo D, Smith N, Liu X-M, Lamberty B, Morsey B, Fox HS, McMillan J, Gendelman HE, Alnouti Y. 2013. Preclinical

AAC

pharmacokinetics and tissue distribution of long-acting nanoformulated antiretroviral therapy. Antimicrob Agents Chemother 57:3110–3120.

20. Song S, Ji Y, Zhang G, Zhang X, Li B, Li D, Jiang W. 2018. Protective Effect of Atazanavir Sulphate Against Pulmonary Fibrosis In Vivo and In Vitro. Basic Clin Pharmacol Toxicol 122:199–207.

21. Wang M, Cao R, Zhang L, Yang X, Liu J, Xu M, Shi Z, Hu Z, Zhong W, Xiao G. 2020. Remdesivir and chloroquine effectively inhibit the recently emerged novel coronavirus (2019-nCoV) in vitro. Cell Res 30:269–271.

22. Zhou F, Yu T, Du R, Fan G, Liu Y, Liu Z, Xiang J, Wang Y, Song B, Gu X, Guan L, Wei Y, Li H, Wu X, Xu J, Tu S, Zhang Y, Chen H, Cao B. 2020. Clinical course and risk factors for mortality of adult inpatients with COVID-19 in Wuhan, China: a retrospective cohort study. The Lancet 395:1054–1062.

23. Newton AH, Cardani A, Braciale TJ. 2016. The host immune response in respiratory virus infection: balancing virus clearance and immunopathology. Semin Immunopathol 38:471–482.

24. Solomon T, Baylis M, Brown D. 2016. Zika virus and neurological disease-approaches to the unknown. Lancet Infect Dis 16:402–4.

25. de Freitas CS, Higa LM, Sacramento CQ, Ferreira AC, Reis PA, Delvecchio R, Monteiro FL, Barbosa-Lima G, James Westgarth H, Vieira YR, Mattos M, Rocha N, Hoelz LVB, Leme RPP, Bastos MM, L Rodrigues GO, M Lopes CE, Queiroz-Junior CM, Lima CX, Costa VV, Teixeira MM, Bozza FA, Bozza PT, Boechat N, Tanuri A,

AAC

Souza TML. 2019. Yellow fever virus is susceptible to sofosbuvir both in vitro and in vivo. PLoS Negl Trop Dis 13:e0007072.

26. Ferreira AC, Reis PA, de Freitas CS, Sacramento CQ, Villas Boas Hoelz L, Bastos MM, Mattos M, Rocha N, Gomes de Azevedo Quintanilha I, da Silva Gouveia Pedrosa C, Rocha Quintino Souza L, Correia Loiola E, Trindade P, Rangel Vieira Y, Barbosa-Lima G, de Castro Faria Neto HC, Boechat N, Rehen SK, Bruning K, Bozza FA, Bozza PT, Souza TML. 2018. Beyond members of the Flaviviridae family, sofosbuvir also inhibits chikungunya virus replication. Antimicrob Agents Chemother 63: e01389-18.

27. Ferreira AC, Zaverucha-do-Valle C, Reis PA, Barbosa-Lima G, Vieira YR, Mattos M, Silva P de P, Sacramento C, Neto HCCF, Campanati L, Tanuri A, Brüning K, Bozza FA, Bozza PT, Souza TML. 2017. Sofosbuvir protects Zika virus-infected mice from mortality, preventing short- and long-term sequelae. Sci Rep 7:9409.

28. Sacramento CQ, de Melo GR, de Freitas CS, Rocha N, Hoelz LV, Miranda M, Fintelman-Rodrigues N, Marttorelli A, Ferreira AC, Barbosa-Lima G, Abrantes JL, Vieira YR, Bastos MM, de Mello Volotão E, Nunes EP, Tschoeke DA, Leomil L, Loiola EC, Trindade P, Rehen SK, Bozza FA, Bozza PT, Boechat N, Thompson FL, de Filippis AM, Brüning K, Souza TM. 2017. The clinically approved antiviral drug sofosbuvir inhibits Zika virus replication. Sci Rep 7:40920.

29. Figueiredo-Mello C, Casadio LVB, Avelino-Silva VI, Yeh-Li H, Sztajnbok J, Joelsons D, Antonio MB, Pinho JRR, Malta F de M, Gomes-Gouvêa MS, Salles APM, Corá AP, Moreira CHV, Ribeiro AF, Nastri AC de SS, Malaque CMS, Teixeira

AAC

RFA, Borges LMS, Gonzalez MP, Junior LCP, Souza TNL, Song ATW, D'Albuquerque LAC, Abdala E, Andraus W, Martino RB de, Ducatti L, Andrade GM, Malbouisson LMS, Souza IM de, Carrilho FJ, Sabino EC, Levin AS. 2019. Efficacy of sofosbuvir as treatment for yellow fever: protocol for a randomised controlled trial in Brazil (SOFFA study). BMJ Open 9:e027207.

30. No clinical benefit from use of lopinavir-ritonavir in hospitalised COVID-19 patients studied in RECOVERY — RECOVERY Trial. https://www.recoverytrial.net/news/no-clinical-benefit-from-use-of-lopinavir-ritonavir-in-hospitalised-covid-19-patients-studied-in-recovery, accessed on 24-jul-2020

31. Hung IF-N, Lung K-C, Tso EY-K, Liu R, Chung TW-H, Chu M-Y, Ng Y-Y, Lo J, Chan J, Tam AR, Shum H-P, Chan V, Wu AK-L, Sin K-M, Leung W-S, Law W-L, Lung DC, Sin S, Yeung P, Yip CC-Y, Zhang RR, Fung AY-F, Yan EY-W, Leung K-H, Ip JD, Chu AW-H, Chan W-M, Ng AC-K, Lee R, Fung K, Yeung A, Wu T-C, Chan JW-M, Yan W-W, Chan W-M, Chan JF-W, Lie AK-W, Tsang OT-Y, Cheng VC-C, Que T-L, Lau C-S, Chan K-H, To KK-W, Yuen K-Y. 2020. Triple combination of interferon beta-1b, lopinavir–ritonavir, and ribavirin in the treatment of patients admitted to hospital with COVID-19: an open-label, randomised, phase 2 trial. The Lancet 395:1695–1704.

32. Cai Q, Yang M, Liu D, Chen J, Shu D, Xia J, Liao X, Gu Y, Cai Q, Yang Y, Shen C, Li X, Peng L, Huang D, Zhang J, Zhang S, Wang F, Liu J, Chen L, Chen S, Wang Z, Zhang Z, Cao R, Zhong W, Liu Y, Liu L. 2020. Experimental Treatment with Favipiravir for COVID-19: An Open-Label Control Study. Engineering.

AAC

33. Sheahan TP, Sims AC, Leist SR, Schäfer A, Won J, Brown AJ, Montgomery SA, Hogg A, Babusis D, Clarke MO, Spahn JE, Bauer L, Sellers S, Porter D, Feng JY, Cihlar T, Jordan R, Denison MR, Baric RS. 2020. Comparative therapeutic efficacy of remdesivir and combination lopinavir, ritonavir, and interferon beta against MERS-CoV. 1. Nat Commun 11:1–14.

34. Lv Z, Chu Y, Wang Y. 2015. HIV protease inhibitors: a review of molecular selectivity and toxicity. HIVAIDS Auckl NZ 7:95–104.

35. Huang J, Gautam N, Bathena SPR, Roy U, McMillan J, Gendelman HE, Alnouti Y. 2011. UPLC-MS/MS quantification of nanoformulated ritonavir, indinavir, atazanavir, and efavirenz in mouse serum and tissues. J Chromatogr B Analyt Technol Biomed Life Sci 879:2332–2338.

36. Beck BR, Shin B, Choi Y, Park S, Kang K. 2020. Predicting commercially available antiviral drugs that may act on the novel coronavirus (2019-nCoV), Wuhan, China through a drug-target interaction deep learning model. bioRxiv 2020.01.31.929547.

37. Yang H, Yang M, Ding Y, Liu Y, Lou Z, Zhou Z, Sun L, Mo L, Ye S, Pang H, Gao GF, Anand K, Bartlam M, Hilgenfeld R, Rao Z. 2003. The crystal structures of severe acute respiratory syndrome virus main protease and its complex with an inhibitor. Proc Natl Acad Sci U S A 100:13190–13195.

38. Macchiagodena M, Pagliai M, Procacci P. 2020. Inhibition of the Main Protease 3CL-pro of the Coronavirus Disease 19 via Structure-Based Ligand Design and Molecular Modeling.

39. Gao R, Bhatnagar J, Blau DM, Greer P, Rollin DC, Denison AM, Deleon-Carnes M, Shieh WJ, Sambhara S, Tumpey TM, Patel M, Liu L, Paddock C, Drew C, Shu Y, Katz JM, Zaki SR. 2013. Cytokine and chemokine profiles in lung tissues from fatal cases of 2009 pandemic influenza A (H1N1): role of the host immune response in pathogenesis. Am J Pathol 183:1258–68.

40. Peschke T, Bender A, Nain M, Gemsa D. 1993. Role of macrophage cytokines in influenza A virus infections. Immunobiology 189:340–55.

41. Channappanavar R, Perlman S. 2017. Pathogenic human coronavirus infections: causes and consequences of cytokine storm and immunopathology. Semin Immunopathol 39:529–539.

42. Monteerarat Y, Sakabe S, Ngamurulert S, Srichatraphimuk S, Jiamtom W, Chaichuen K, Thitithanyanont A, Permpikul P, Songserm T, Puthavathana P, Nidom CA, Mai le Q, Iwatsuki-Horimoto K, Kawaoka Y, Auewarakul P. 2010. Induction of TNF-alpha in human macrophages by avian and human influenza viruses. Arch Virol 155:1273–9.

43. Reed H LJ,& Muench. 1938. A simple method of estimating fifty percent endpoints. Am J Hyg.

44. CDC. 2020. Coronavirus Disease 2019 (COVID-19). Cent Dis Control Prev.

45. Jakalian A, Jack DB, Bayly CI. 2002. Fast, efficient generation of high-quality atomic charges. AM1-BCC model: II. Parameterization and validation. J Comput Chem 23:1623–1641.

AAC

46. Wang J, Wolf RM, Caldwell JW, Kollman PA, Case DA. 2004. Development and testing of a general amber force field. J Comput Chem 25:1157–1174.

47. Allen WJ, Balius TE, Mukherjee S, Brozell SR, Moustakas DT, Lang PT, Case DA, Kuntz ID, Rizzo RC. 2015. DOCK 6: Impact of new features and current docking performance. J Comput Chem 36:1132–1156.

48. Jin Z, Du X, Xu Y, Deng Y, Liu M, Zhao Y, Zhang B, Li X, Zhang L, Duan Y, Yu J, Wang L, Yang K, Liu F, You T, Liu X, Yang X, Bai F, Liu H, Liu X, Guddat LW, Xiao G, Qin C, Shi Z, Jiang H, Rao Z, Yang H. 2020. Structure-based drug design, virtual screening and high-throughput screening rapidly identify antiviral leads targeting COVID-19. bioRxiv 2020.02.26.964882.

49. Pettersen EF, Goddard TD, Huang CC, Couch GS, Greenblatt DM, Meng EC, Ferrin TE. 2004. UCSF Chimera--a visualization system for exploratory research and analysis. J Comput Chem 25:1605–1612.

50. Phillips JC, Braun R, Wang W, Gumbart J, Tajkhorshid E, Villa E, Chipot C, Skeel RD, Kalé L, Schulten K. 2005. Scalable molecular dynamics with NAMD. J Comput Chem 26:1781–1802.

51. MacKerell AD, Banavali N, Foloppe N. 2000. Development and current status of the CHARMM force field for nucleic acids. Biopolymers 56:257–265.

52. Zhang T, Nguyen PH, Nasica-Labouze J, Mu Y, Derreumaux P. 2015. Folding Atomistic Proteins in Explicit Solvent Using Simulated Tempering. J Phys Chem B 119:6941–6951.

53. Hoang Viet M, Derreumaux P, Nguyen PH. 2015. Communication: Multiple atomistic force fields in a single enhanced sampling simulation. J Chem Phys 143:021101.

54. Lindorff-Larsen K, Piana S, Dror RO, Shaw DE. 2011. How fast-folding proteins fold. Science 334:517–520.

55. Jorgensen WL, Chandrasekhar J, Madura JD, Impey RW, Klein ML. 1998. Comparison of simple potential functions for simulating liquid water.

56. Darden T, York D, Pedersen L. 1993. Particle mesh Ewald: An N·log(N) method for Ewald sums in large systems. J Chem Phys 98:10089–10092.

57. Heussen C, Dowdle EB. 1980. Electrophoretic analysis of plasminogen activators in polyacrylamide gels containing sodium dodecyl sulfate and copolymerized substrates. Anal Biochem 102:196–202.

58. Alves CR, Marzochi MC, Giovanni-de-Simone S. 1993. Heterogeneity of cysteine proteinases in Leishmania braziliensis and Leishmania major. Braz J Med Biol Res Rev Bras Pesqui Medicas E Biol 26:167–171.

Author contributions

Experimental execution and analysis – NFR, CQS, CRL, FSS, ACF, MM, MM, CSF, VCS, SSGD, JRT, MDM, ARM

Data analysis, manuscript preparation and revision – NFR, CQS, ACF, CSF, CRL, FSS, FAB, NC, CRA, MMS, PTB, TMLS

Conceptualized the experiments – NFR, CQS, TMLS

Study coordination – TMLS

Manuscript preparation and revision – PTB, TMLS

The authors declare no competing financial interests.

Legend for the Figures

Figure 1. **Final positions of ATV and LPV on Mpro at the end of a molecular dynamic simulation.** Representative images of LPV (A; blue estructure) and ATV (B; orange structure) positioned in the Mpro (green). Two-dimensional (2D) representation of the interactions of LPV (C) and ATV (D) in the Mpro active site at the end of 100 ns molecular dynamic simulation.

Figure 2. Inhibition of proteinase activity through an analysis of gelatinolytic activity. Vero cells were mock treated or infected with SARS-CoV-2 at an MOI of 0.1 for 48h before lysis and preparation of a cellular fraction. Fractions containing 12 µg of total protein separated by electrophoresis followed by cutting the gels into their individual lanes that were incubated in 10 mM sodium acetate buffer (pH 5.5) in the absence (Nil) or presence of 10 µM of E-64, ATV or RTV. Gelatinolytic bands indicative of enzymatic activity were revealed by negative staining with amide black solution. Molecular mass markers are indicated (kDa).

Figure 3. The antiviral activity of ATV and ATV/RTV against SARS-CoV-2. Vero (A and B) or A549 (C) cells were infected with SARS-CoV-2 at the MOI of 0.01 and exposed to indicated concentrations of atazanavir (ATV), atazanavir/ritonavir (ATV/RTV; 3:1), chloroquine (CQ), remsedivir (RDV) or lopinavir/ritonavir (LPV/RTV; 4:1). After 2 days, the viral replication in the culture supernatant was measured by $TCID_{50}$/mL (A) or RT-PCR (B and C). The data represent means ± SEM of three independent experiments.

Figure 4. ATV and ATV/RTV impairs SARS-CoV-2 replication, cell death and cytokine storm in human primary monocytes. Human primary monocytes were infected

AAC

at the indicated MOI of 0.01 and treated with indicated concentration of atazanavir (ATV), atazanavir/ritonavir (ATV/RTV; 3:1), chloroquine (CQ), remsedivir (RDV) or lopinavir/ritonavir (LPV/RTV; 4:1). After 24h, cell-associated subgenomic RNA levels (A) and LDH release (B) as well as the levels of IL-6 (C) and TNF-α (D) were measured in the culture supernatant. The data represent means ± SD of experiments with cells from at least three healthy donors. Differences with $P < 0.05$ are indicates (*), when compared to untreated cells (nil).

AAC

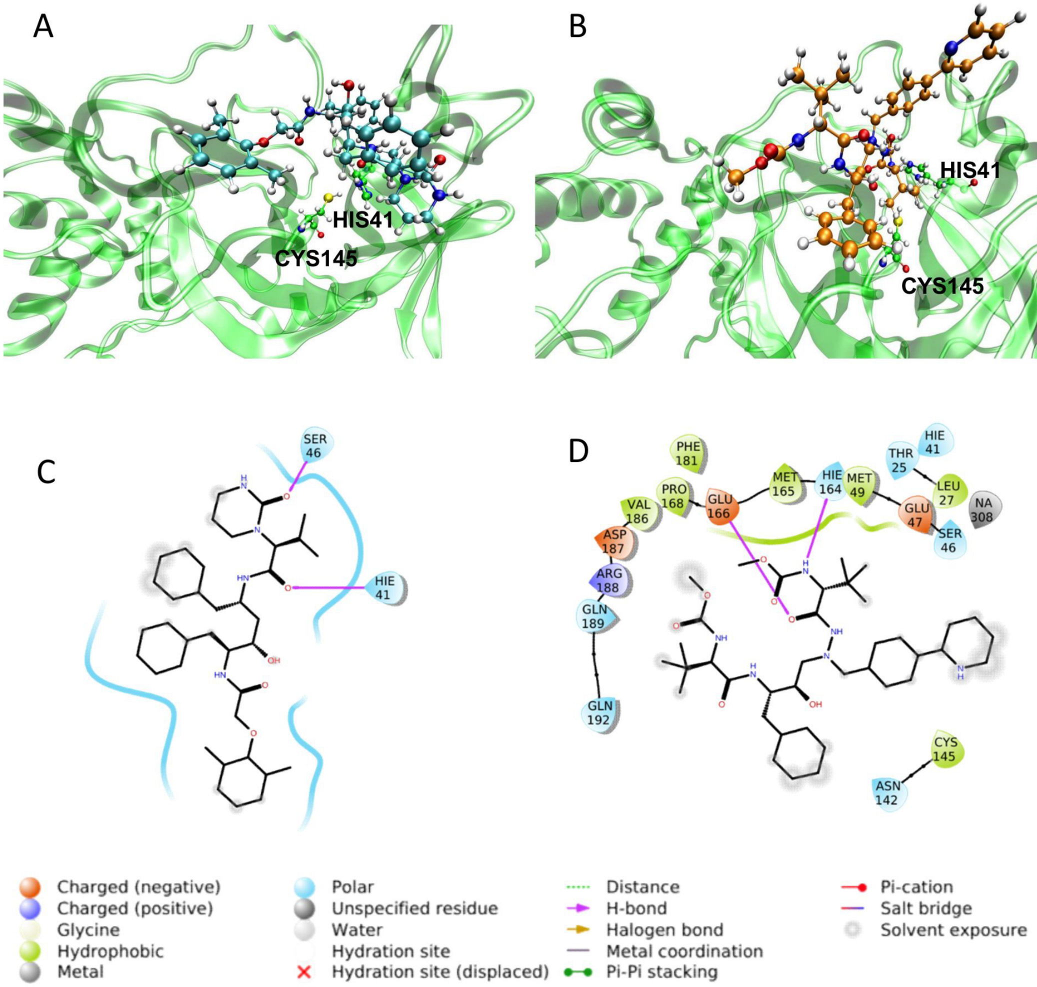
A
HIS41
CYS145
B
HIS41
CYS145
C
SER 46
HIE 41
D
PHE 181
PRO 168
VAL 186
ASP 187
ARG 188
GLN 189
GLN 192
GLU 166
MET 165
HIE 164
MET 49
THR 25
HIE 41
LEU 27
NA 308
GLU 47
SER 46
CYS 145
ASN 142
Charged (negative)
Charged (positive)
Glycine
Hydrophobic
Metal
Polar
Unspecified residue
Water
Hydration site
Hydration site (displaced)
Distance
H-bond
Halogen bond
Metal coordination
Pi-Pi stacking
Pi-cation
Salt bridge
Solvent exposure

AAC

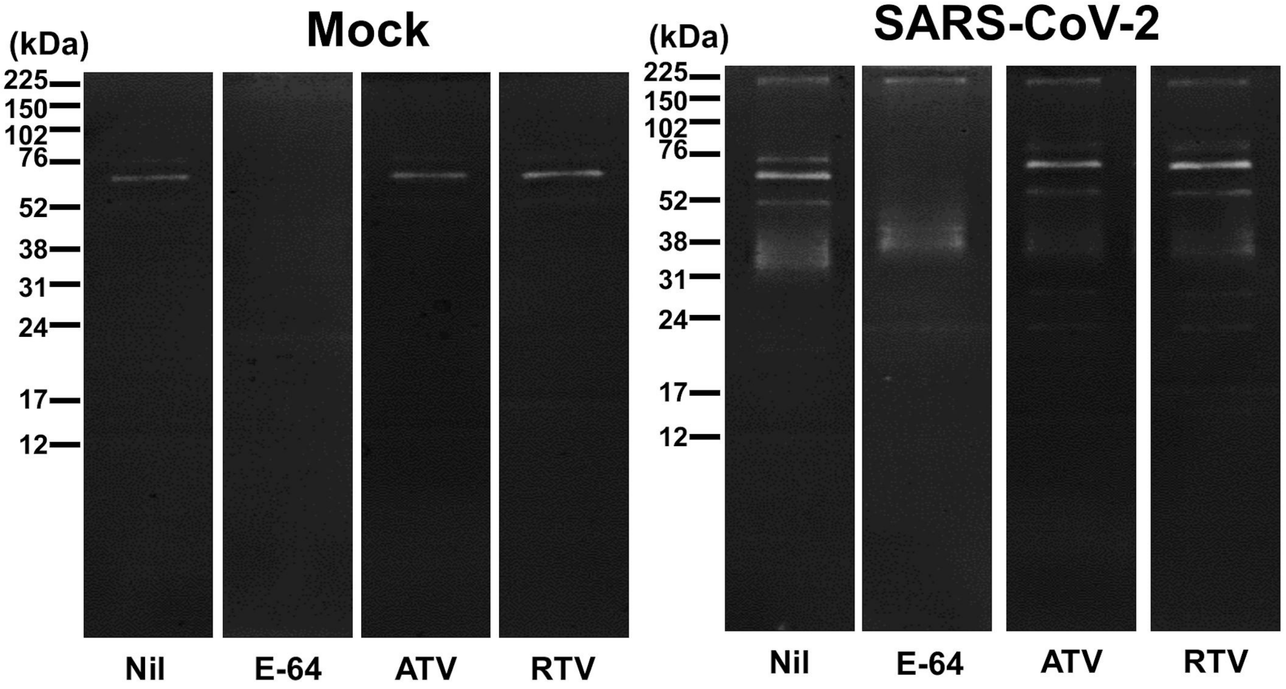
Mock
(kDa)
225
150
102
76
52
38
31
24
17
12
Nil
E-64
ATV
RTV
SARS-CoV-2
(kDa)
225
150
102
76
52
38
31
24
17
12
Nil
E-64
ATV
RTV

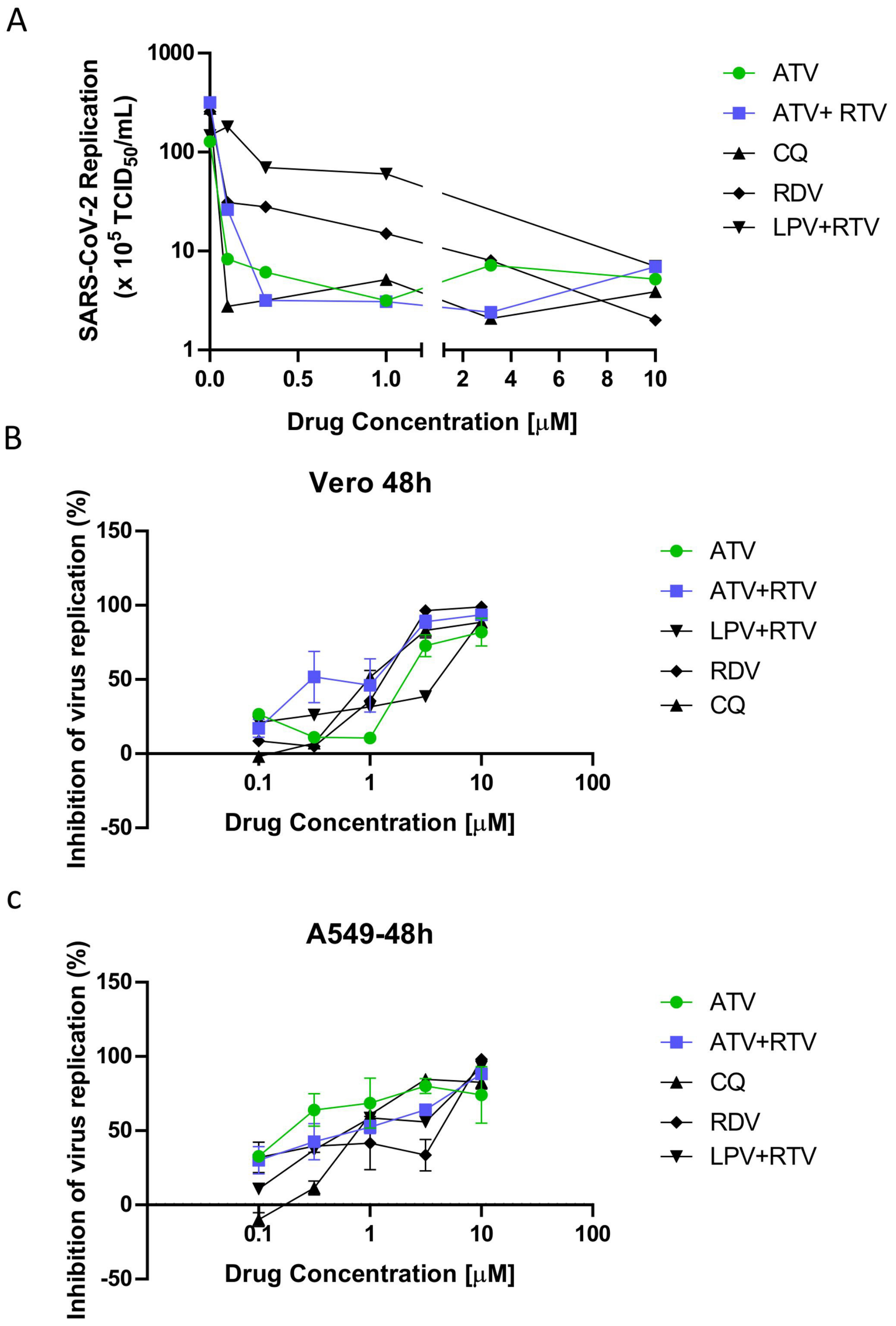
A
SARS-CoV-2 Replication
(x 10^5 $TCID_{50}$/mL)
1000
100
10
1
0.0
0.5
1.0
2
4
6
8
10
Drug Concentration [μM]
ATV
ATV+ RTV
CQ
RDV
LPV+RTV
B
Vero 48h
Inhibition of virus replication (%)
150
100
50
0
-50
0.1
1
10
100
Drug Concentration [μM]
ATV
ATV+RTV
LPV+RTV
RDV
CQ
C
A549-48h
Inhibition of virus replication (%)
150
100
50
0
-50
0.1
1
10
100
Drug Concentration [μM]
ATV
ATV+RTV
CQ
RDV
LPV+RTV

AAC

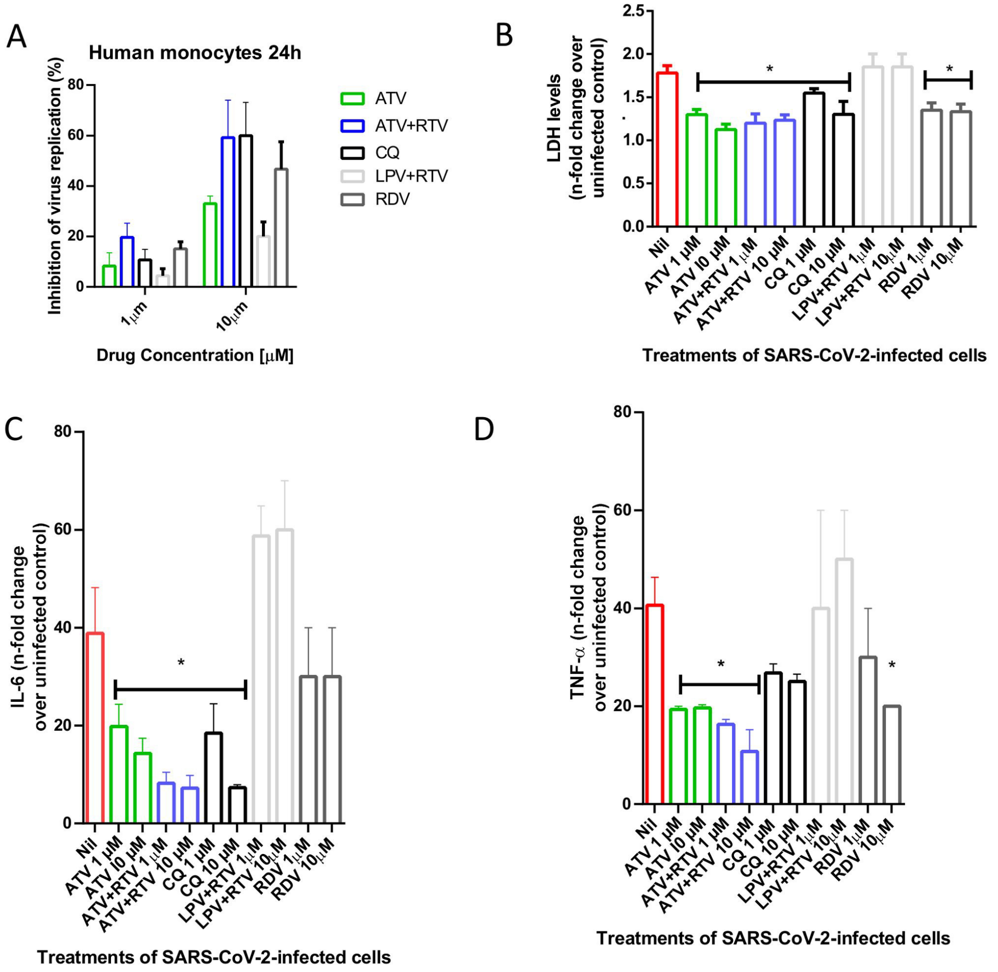
A
Human monocytes 24h
Inhibition of virus replication (%)
0
20
40
60
80
1μm
10μm
Drug Concentration [μM]
ATV
ATV+RTV
CQ
LPV+RTV
RDV
B
LDH levels
(n-fold change over
uninfected control)
0.0
0.5
1.0
1.5
2.0
2.5
*
*
Nil
ATV 1 μM
ATV 10 μM
ATV+RTV 1 μM
ATV+RTV 10 μM
CQ 1 μM
CQ 10 μM
LPV+RTV 1μM
LPV+RTV 10μM
RDV 1μM
RDV 10μM
Treatments of SARS-CoV-2-infected cells
C
IL-6 (n-fold change
over uninfected control)
0
20
40
60
80
*
Nil
ATV 1 μM
ATV 10 μM
ATV+RTV 1 μM
ATV+RTV 10 μM
CQ 1 μM
CQ 10 μM
LPV+RTV 1μM
LPV+RTV 10μM
RDV 1μM
RDV 10μM
Treatments of SARS-CoV-2-infected cells
D
TNF-α (n-fold change
over uninfected control)
0
20
40
60
80
*
*
Nil
ATV 1 μM
ATV 10 μM
ATV+RTV 1 μM
ATV+RTV 10 μM
CQ 1 μM
CQ 10 μM
LPV+RTV 1μM
LPV+RTV 10μM
RDV 1μM
RDV 10μM
Treatments of SARS-CoV-2-infected cells

AAC